JAERI-Research
2000-023

A SPATIAL DISCRETIZATION OF THE MHD EQUATIONS BASED ON THE FINITE VOLUME - SPECTRAL METHOD

May 2000

Takahiro MIYOSHI and NEXT Group

日本原子力研究所
Japan Atomic Energy Research Institute

本レポートは，日本原子力研究所が不定期に公刊している研究報告書です。
入手の問合わせは，日本原子力研究所研究情報部研究情報課（〒319-1195　茨城県那珂郡東海村）あて，お申し越しください。なお，このほかに財団法人原子力弘済会資料センター（〒319-1195　茨城県那珂郡東海村日本原子力研究所内）で複写による実費頒布をおこなっております。

This report is issued irregularly.
Inquiries about availability of the reports should be addressed to Research Information Division, Department of Intellectual Resources, Japan Atomic Energy Research Institute, Tokai-mura, Naka-gun, Ibaraki-ken, 319-1195, Japan.

編集兼発行　　日本原子力研究所

JAERI-Research 2000-023

A Spatial Discretization of the MHD Equations Based on the Finite Volume - Spectral Method

Takahiro Miyoshi and NEXT Group

Department of Fusion Plasma Research
Naka Fusion Research Establishment
Japan Atomic Energy Research Institute
Naka-machi, Naka-gun, Ibaraki-ken

(Received April 5, 2000)

Based on the finite volume - spectral method, we present new discretization formulae for the spatial differential operators in the full system of the compressible MHD equations. In this approach, the cell-centered finite volume method is adopted in a bounded plane (poloidal plane), while the spectral method is applied to the differential with respect to the periodic direction perpendicular to the poloidal plane (toroidal direction). Here, an unstructured grid system composed of the arbitrary triangular elements is utilized for constructing the cell-centered finite volume method. In order to maintain the divergence free constraint of the magnetic field numerically, only the poloidal component of the rotation is defined at three edges of the triangular element. This poloidal component is evaluated under the assumption that the toroidal component of the operated vector times the radius, RA_ϕ, is linearly distributed in the element. The present method will be applied to the nonlinear MHD dynamics in an realistic torus geometry without the numerical singularities.

Keywords: MHD Simulation, Finite Volume Method, Spectral Method, Compressibility

有限体積–スペクトル法によるMHD方程式の離散化

日本原子力研究所那珂研究所炉心プラズマ研究部

三好 隆博・NEXTグループ

(2000年4月5日 受理)

有限体積–スペクトル法に基づく圧縮性MHD方程式の離散化公式を提出する。本手法では、ポロイダル断面においては体積中心有限体積法を、周期性を持つトロイダル方向に関してはスペクトル法を適用する。体積中心有限体積法に対しては、任意の三角形要素で構成された非構造格子が利用された。ただし、磁場の発散がゼロという拘束条件を数値的に満足し続けるよう、回転演算子のポロイダル成分に関してのみ、三角形要素辺の中点に定義した。ここでは、被演算ベクトルのトロイダル成分と半径との積(RA_ϕ)が三角形要素内で線形に分布していると仮定し、回転演算子のポロイダル成分の評価を行なった。本離散化手法を利用することにより、実形状トーラスプラズマにおけるMHDシミュレーションが、数値的な特異性無く実行可能になると期待される。

那珂研究所：〒311-0193 茨城県那珂郡那珂町向山801-1

Contents

1. Introduction 1

2. Basic Equations 2

3. Discretization of Differential Operators 3

3.1. Gradient of Scalar (∇f) 3
3.2. Divergence of Vector ($\nabla \cdot \mathbf{A}$) 4
3.3. Divergence of Tensor ($\nabla \cdot \mathbf{T}$) 5
3.4. Gradient of Vector ($\nabla \mathbf{A}$) 5
3.5. Rotation of Vector ($\nabla \times \mathbf{A}$) 5
3.5.1. Toroidal Component 6
3.5.2. Poloidal Component (Normal Component) 6
3.5.3. Poloidal Component (Tangential Component) 7
3.5.4. Divergence of Discretized Rotation 9

4. Boundary Conditions 9

5. Summary 9

Acknowledgment 10

References 10

目次

1. 序論 1
2. 基礎方程式 2
3. 微分演算子の離散化 3
3.1. スカラー勾配 (∇f) 3
3.2. ベクトル発散 ($\nabla \cdot \mathbf{A}$) 4
3.3. テンソル発散 ($\nabla \cdot \mathbf{T}$) 5
3.4. ベクトル勾配 ($\nabla \mathbf{A}$) 5
3.5. ベクトル回転 ($\nabla \times \mathbf{A}$) 5
3.5.1. トロイダル成分 6
3.5.2. ポロイダル成分 (垂直成分) 6
3.5.3. ポロイダル成分 (接線成分) 7
3.5.4. 離散回転演算子の発散 9
4. 境界条件 9
5. まとめ 9
謝辞 10
参考文献 10

1. Introduction

The magnetohydrodynamics (MHD), which describes a macroscopic plasma dynamics accompanied with the global magnetic activity, has been deeply studied in various research fields such as fusion, space, or astrophysical plasma researches. Especially, in order to clarify the complex dynamics of the nonlinear MHD, the MHD simulations have been performed for the last few decades. In space plasma researches, for instance, the global MHD simulations of the planetary magnetosphere (e.g., for the Earth's magnetosphere [1], or for the Jovian magnetosphere [2]) were performed as a powerful means of studying the global structure and dynamics of the solar wind - magnetosphere interaction. Also, in fusion plasma researches, the nonlinear MHD simulations were presented to illuminate the dynamic activities in various fusion devices; collapse events in the tokamak [3-5], the self-reversal process in the reversed field pinch (RFP) [6], the internal reconnection event in the spherical tokamak (ST) [7], and so on. The approaches of those simulations are roughly classified into two types as follows: One type is that the equations are discretized on the grid aligned with the circular or the concentric flux coordinate. Therefore, a realistic machine geometry as well as a separatrix configuration cannot be treated in the numerical simulation though the higher-order accuracy is realized by the spectral method for both the toroidal and the poloidal directions. Also, even when we consider an ideal concentric configuration, the violent nonlinear dynamics of the non-ideal MHD largely shifts the magnetic field from the initial flux coordinate, and as a result, breaks the calculation. On the other hand, in the other type, a finite difference method on the cartesian grid is applied in the rectangular poloidal plane. Thus, the violent MHD phenomena in the fusion reactor may be simulated without numerical instabilities if we choose proper numerical scheme. However, this approach leads to less accuracy than the above spectral method. It is also natural that this is inadequate for the simulation in a realistic geometry.

In the research fields of the fluid mechanics, large scale computer simulations have greatly progressed in a frontier field as the computational fluid dynamics (CFD). Especially, in the view point of a design on airplane, automobile, and so on, the simulations on the unstructured grid, which is composed of various geometric elements, have been developed to a high degree in the CFD to fit the complicated boundary geometry. The other advantage of the simulations on the unstructured grid is that, due to the absence of the regularity for the grid structure, the elements can be readily concentrated on desirable locations where the finer structures appear. On this unstructured grid, we can construct a numerical scheme based on the alternative of the finite element method, where the equations cannot be discretized not by a variational principle but by the method of weighted residuals in general, or the finite volume method, in which the integral form of the conservation laws are discretized directly. Quite recently, also for the MHD researches, these two approaches, the finite element method [8,9] and the finite volume method [10], were introduced separately in order to simulate the nonlinear dynamics of torus plasma. Here we note that, for both approaches, the spectral method is applied to the toroidal direction due to the periodicity of the torus geometry. The compressible MHD simulation by means of those numerical techniques becomes quite important to comprehend the mechanism of the violent dynamics in high beta torus plasmas within the realistic geometry.

Through the one of those approaches, the finite volume method [10], we can naturally introduce the discretization which satisfy the divergence free condition of the magnetic filed. Therefore, in this paper, we present a variant of discretization formulae for the whole first-order differential operator appearing in the full system of the compressible MHD equations based on the finite volume - spectral method. The finite volume method is adopted in a two dimensional plane while the spectral method is applied to the one dimensional periodic direction perpendicular to that plane. The higher-order differential operators related to the dissipative term in the MHD equations are evaluated from the first-order operators in this study. Particularly, in order

to simulate the dynamics of high beta plasma in fusion reactors, we present a suitable form of the compressible MHD equations for such problems in sections 2. In section 3, every differential operator appearing in the MHD equations is discretized explicitly. The boundary condition for the present discretization is mentioned in section4. Finally, we summarize the results of this paper in section 5.

2. Basic Equations

The full system of the compressible MHD equations as well as the compressible Navier-Stokes equations can be written in the conservative form. Therefore, the integral form of these equations may have the discontinuous solutions. Indeed, it has been well known from the MHD studies of the planetary magnetosphere that discontinuities such as the bow shock and the magnetopause appear in the sun side of the magnetosphere due to the interaction with the supersonic solar wind. In order to capture such discontinuities numerically, the conservative form of the MHD equations has been directly discretized in which the numerical fluxes at the cell boundary are estimated by the upwind-weighted fluxes for instance [2]. However, the discretization for the conservative form of the compressible MHD equations, particularly in the low beta situation, may produce large numerical errors in the energy equation and lead an incorrect Lorentz force toward the magnetic field in the momentum equation. In the incompressible MHD simulations such as the studies for the MHD turbulence, on the other hand, the flux function - stream function form in two dimensions [11] or the non-conservative form in three dimensions [12] was often used as the discretized form of the MHD equations, where the pressure is determined to satisfy the divergence free constraint of the velocity field. Also, tokamak simulations have been performed under the reduced MHD approximation where the flux function - stream function form is discretized by some manners [13].

Recently, as an effective approach for the global MHD simulation of the Earth's magnetosphere, the direct discretization for the semi-conservative form of the compressible MHD equations was proposed to simulate the dynamics of both extremely high and low beta plasmas in the magnetospheric system [14]. Similarly, in order to clarify the dynamics of high beta fusion plasmas that is appropriate for the middle range of beta in the global magnetospheric simulation, we discretize the semi-conservative form of the compressible MHD equations as follows:

$$\frac{\partial \rho}{\partial t} = -\nabla \cdot (\rho \mathbf{V}), \tag{1}$$

$$\frac{\partial (\rho \mathbf{V})}{\partial t} = -\nabla \cdot (\rho \mathbf{V}\mathbf{V} + P\mathbf{I} + \mathbf{\Pi}) + \mathbf{J} \times \mathbf{B}, \tag{2}$$

$$\frac{\partial \epsilon_F}{\partial t} = -\nabla \cdot [(\epsilon_F + P)\mathbf{V} + \mathbf{\Pi} \cdot \mathbf{V}] + \mathbf{J} \cdot \mathbf{E}, \tag{3}$$

$$\frac{\partial \mathbf{B}}{\partial t} = -\nabla \times \mathbf{E}, \tag{4}$$

where ρ, $\mathbf{V}$, ϵ_F, $\mathbf{B}$, P, $\mathbf{\Pi}$, $\mathbf{J}$, $\mathbf{E}$, and $\mathbf{I}$ denote the plasma density, the bulk velocity, the fluid energy density, the magnetic field, the plasma pressure, the viscous tensor, the current density, the electric field, and the unit matrix, respectively. The relations between the time dependent variables at the left-hand side of the above equations and other variables can be written as

$$\epsilon_F = \frac{P}{\gamma - 1} + \frac{1}{2}\rho V^2, \tag{5}$$

$$\mathbf{\Pi} = \nu[\frac{2}{3}(\nabla \cdot \mathbf{V})\mathbf{I} - \nabla \mathbf{V} - {}^t(\nabla \mathbf{V})], \tag{6}$$

$$\mathbf{E} = -\mathbf{V} \times \mathbf{B} + \eta \mathbf{J}, \tag{7}$$

$$\mathbf{J} = \frac{1}{\mu_0}\nabla \times \mathbf{B}, \tag{8}$$

where γ, ν, η, and μ_0 indicate the adiabatic constant, the viscosity, the resistivity, and the permeability, respectively. Here the viscous tensor is obtained under the collision-dominated assumption. The fluid equations from (1) to (3) are written by the conservative form of the fluid components with the the electromagnetic terms as the source terms. From these equations, we can construct a numerical scheme based on the finite volume method such that the volume integral of the density, the momentum and the energy density are exactly conserved without the source terms. Also, a scheme which conserves the total magnetic flux can be constructed.

3. Discretization of Differential Operators

As seen in the previous section, the operators in the full system of the compressible MHD equations are given by the gradient of a scalar, the divergence of a vector, the divergence of a tensor, and the rotation of a vector. Additionally, in order to estimate the viscous tensor, the gradient of a vector must be considered. These differential operators will be discretized both by the finite volume method in the poloidal plane and by the spectral method for the differential with respect to the toroidal direction in the torus geometry as shown in Figure 1 or in the general geometry periodic at least for one direction. Here, the poloidal plane is composed of the arbitrary triangular elements as seen in Figure 1(b) where the triangles are given by Delaunay triangles, for example. Since we decompose a function f (or $\mathbf{A}$ for a vector function) into a series of which $f(R,\phi,z) = \sum_n \tilde{f}(R,z)_n e^{\mathcal{I}n\phi}$ (n: the toroidal mode number; $\mathcal{I}$: the imaginary unit), the differential of the scalar (vector) function to the toroidal direction is replaced by the complex scalar (vector). As a result, the numerical scheme constructed here is regarded as the two dimensional finite volume method for the complex MHD equations including the curvature effect of the torus geometry. In the followings, we specify the discretization formulae for the operators.

3.1. Gradient of Scalar (∇f)

The averaged gradient of f in the volume element denoted by i is defined as

$$\begin{aligned}
&\int_{V_i|_{\Delta\phi\to 0}} (\nabla f) dV \\
&= \sum_n \int_0^{\Delta\phi} e^{\mathcal{I}n\phi} d\phi \int_{S_i} R(\widetilde{\nabla f})_n dS \\
&= \sum_n \Delta\phi R_i (\widetilde{\nabla f})_{i,n} S_i,
\end{aligned} \tag{9}$$

where S_i and R_i are the area of the triangular element, $\int_{S_i} dS$, and R coordinate of the centroid of the triangle, $\int_{S_i} RdS/S_i$, respectively. On the other hand, the alternative of the surface integral formula of the gradient for the torus configuration can be written as

$$\begin{aligned}
&\int_{V_i|_{\Delta\phi\to 0}} (\nabla f) dV \\
&= \int_0^{\Delta\phi} \int_{z_{S_i}} \int_{R_{S_i}} (R\nabla f) dR dz d\phi \\
&= \int_0^{\Delta\phi} \int_{z_{S_i}} \int_{R_{S_i}} (R\frac{\partial f}{\partial R}\mathbf{e}_R + \frac{\partial f}{\partial \phi}\mathbf{e}_\phi + R\frac{\partial f}{\partial z}\mathbf{e}_z) dR dz d\phi
\end{aligned}$$

$$
\begin{aligned}
&= \int_0^{\Delta\phi}\int_{z_{S_i}}\int_{R_{S_i}}\{(\frac{\partial(Rf)}{\partial R}-f)\mathbf{e}_R+\frac{\partial f}{\partial\phi}\mathbf{e}_\phi+\frac{\partial(Rf)}{\partial z}\mathbf{e}_z\}dRdzd\phi \\
&= \sum_n\int_0^{\Delta\phi}e^{\mathcal{I}n\phi}d\phi\{\int_{z_{S_i}}\int_{R_{S_i}}(\frac{\partial(R\tilde{f}_n)}{\partial R}\mathbf{e}_R+\frac{\partial(R\tilde{f}_n)}{\partial z}\mathbf{e}_z)dRdz \\
&\qquad -\int_{z_{S_i}}\int_{R_{S_i}}\tilde{f}_n dRdz\mathbf{e}_R+\mathcal{I}n\int_{z_{S_i}}\int_{R_{S_i}}\tilde{f}_n dRdz\mathbf{e}_\phi\} \\
&= \sum_n\Delta\phi\{\oint_{l_i}(R\tilde{f}_n\mathbf{n})dl-\int_{S_i}\tilde{f}_n dS_\phi\mathbf{e}_R+\mathcal{I}n\int_{S_i}\tilde{f}_n dS_\phi\mathbf{e}_\phi\},
\end{aligned}
$$

where $\mathbf{n}$, $\mathbf{e}_k$, and (R_{S_i},z_{S_i}) denote the unit vector outwardly normal to the edge, the unit vector in k-direction, and the coordinates in the area, respectively. Also, here, $\oint_{l_i}\cdot\,dl$ indicates the line integral along the triangular edges turning as a left-handed screw to the toroidal direction, i.e., along the unit vector $\mathbf{t}=\mathbf{n}\times\mathbf{e}_\phi$. Thus, the integral form of the gradient f can be discretized as

$$
\int_{V_i|_{\Delta\phi\to 0}}(\nabla f)dV=\sum_n\Delta\phi\{\sum_e R_e\tilde{f}_{e,n}\mathbf{n}_e\Delta l_e-\tilde{f}_{i,n}S_i\mathbf{e}_R+\mathcal{I}n\tilde{f}_{i,n}S_i\mathbf{e}_\phi\}. \tag{10}
$$

Here, subscript e shows the edge of the triangle as depicted in Figure 2, and then, $\tilde{f}_{e,n}$ indicates the n mode numerical flux at the edge. By comparing the n mode component of equations (9) and (10), one can obtain the following discretization formula for ∇f:

$$
\widetilde{(\nabla f)}_{i,n}=\frac{1}{R_iS_i}\sum_e R_e\tilde{f}_{e,n}\mathbf{n}_e\Delta l_e-\frac{1}{R_i}\tilde{f}_{i,n}\mathbf{e}_R+\frac{\mathcal{I}n}{R_i}\tilde{f}_{i,n}\mathbf{e}_\phi. \tag{11}
$$

The toroidal effect appears in all terms at the right-hand side of the above equation. In the limit of the large aspect ratio as $R_0/a\to\infty$ (a: the minor radius; R_0: the major radius), R_e/R_i, $1/R_i$ asymptotically approach 1, 0, respectively, and $\mathcal{I}n/R_i$ is replaced by $\mathcal{I}n$. Thus, the formula without the toroidal effect is reduced as

$$
\widetilde{(\nabla f)}_{i,n}=\frac{1}{S_i}\sum_e\tilde{f}_{e,n}\mathbf{n}_e\Delta l_e+\mathcal{I}n\tilde{f}_{i,n}\mathbf{e}_y, \tag{12}
$$

where the toroidal direction ϕ is replaced by y as a cartesian coordinate. This is equivalent to the two dimensional finite volume method with a correction of adding the n mode term.

In this way, as found from equation (11) or (12), the gradient of a scalar function f in the element i is evaluated both by the operated function $\tilde{f}_{i,n}$ itself and by the numerical fluxes at the triangular edges $\tilde{f}_{e,n}$ where $\tilde{f}_{e,n}\equiv F(\tilde{f}_{i,n},\tilde{f}_{j,n},\cdots)$. Insofar as the property that $\tilde{f}_{i,n}=F(\tilde{f}_{i,n},\tilde{f}_{i,n},\cdots)$ is satisfied, one can choose the evaluated function F arbitrarily. Thus, for instance, we can select the arithmetic mean between $\tilde{f}_{i,n}$ and the neighbor one $\tilde{f}_{j,n}$ in the element j as

$$
\tilde{f}_{e,n}=\frac{1}{2}(\tilde{f}_{i,n}+\tilde{f}_{j,n}),
$$

or the upwind-weighted evaluation to capture the strong shock. When the numerical fluxes are evaluated by the simple arithmetic mean, the gradient of f is calculated only from the discrete functions in and adjacent to the element i.

3.2. Divergence of Vector ($\nabla\cdot\mathbf{A}$)

The divergence of a vector function $\mathbf{A}$ is also discretized by making a comparison between the volume integral form and the surface integral form of the divergence of $\mathbf{A}$. Thus, the discretization formula for $\nabla\cdot\mathbf{A}$ is given by

$$
\widetilde{(\nabla\cdot\mathbf{A})}_{i,n}=\frac{1}{R_iS_i}\sum_e R_e\tilde{\mathbf{A}}_{e,n}\cdot\mathbf{n}_e\Delta l_e+\frac{\mathcal{I}n}{R_i}\widetilde{A_\phi}_{i,n}. \tag{13}
$$

In the absence of the toroidal effect, this formula is reduced as

$$(\widetilde{\nabla \cdot \mathbf{A}})_{i,n} = \frac{1}{S_i} \sum_e \tilde{\mathbf{A}}_{e,n} \cdot \mathbf{n}_e \Delta l_e + \mathcal{I} n \widetilde{A_y}_{i,n}. \tag{14}$$

3.3. Divergence of Tensor $(\nabla \cdot \mathbf{T})$

Following from above manners, the divergence of a tensor $\mathbf{T}$ is discretized as

$$(\widetilde{\nabla \cdot \mathbf{T}})_{i,n} = \frac{1}{R_i S_i} \sum_e R_e \mathbf{n}_e \cdot \tilde{\mathbf{T}}_{e,n} \Delta l_e + \frac{\mathcal{I} n}{R_i} \mathbf{e}_\phi \cdot \tilde{\mathbf{T}}_{i,n} + \frac{1}{R_i} \mathbf{e}_z \times (\mathbf{e}_\phi \cdot \tilde{\mathbf{T}}_{i,n}). \tag{15}$$

Also, in the straight limit, it is written as

$$(\widetilde{\nabla \cdot \mathbf{T}})_{i,n} = \frac{1}{S_i} \sum_e \mathbf{n}_e \cdot \tilde{\mathbf{T}}_{e,n} \Delta l_e + \mathcal{I} n \mathbf{e}_y \cdot \tilde{\mathbf{T}}_{i,n}. \tag{16}$$

It is found that the divergence of the uniform diagonal tensor as $\nabla \cdot (f\mathbf{I})$ strictly corresponds to the discretization formula for the gradient of f as presented in 3.1.

3.4. Gradient of Vector $(\nabla \mathbf{A})$

In addition to the operators discretized above, the gradient of a vector must be also discretized to evaluate the viscous tensor which includes the non-diagonal components for the compressible MHD equations. The formula for the torus version is derived as

$$(\widetilde{\nabla \mathbf{A}})_{i,n} = \frac{1}{R_i S_i} \sum_e R_e \mathbf{n}_e \tilde{\mathbf{A}}_{e,n} \Delta l_e - \frac{1}{R_i} \mathbf{e}_R \tilde{\mathbf{A}}_{i,n} + \frac{\mathcal{I} n}{R_i} \mathbf{e}_\phi \tilde{\mathbf{A}}_{i,n} + \frac{1}{R_i} \mathbf{e}_\phi (\mathbf{e}_z \times \tilde{\mathbf{A}}_{i,n}), \tag{17}$$

while that for the straight version is reduced as

$$(\widetilde{\nabla \mathbf{A}})_{i,n} = \frac{1}{S_i} \sum_e \mathbf{n}_e \tilde{\mathbf{A}}_{e,n} \Delta l_e + \mathcal{I} n \mathbf{e}_y \tilde{\mathbf{A}}_{i,n}. \tag{18}$$

In the latter case, the discretization formula seems to be simple extension of the formula for the gradient of a scalar (12) into a vector.

3.5. Rotation of Vector $(\nabla \times \mathbf{A})$

In the previous discretization, the cell-centered finite volume method where the physical quantities are defined at the centroid of the volume element is applied in the poloidal plane. Although one can also construct such formulae for the rotation operator, the divergence free condition of the rotation as $\nabla \cdot \nabla \times = 0$ cannot be satisfied numerically. Therefore, we introduce another discretization of the finite volume method only for the rotation operator.

For the direct finite difference discretization of the incompressible Navier-Stokes equations, the variables are often defined at a non-collocated grid in order to maintain the divergence free condition of the continuity equation (e.g., well-known MAC method on the staggered grid). Also, in the MHD simulation, a numerical scheme with non-collocated variables, e.g., the constrained transport (CT) scheme [15], has been adopted as a proposed scheme to avoid the generation of the numerical magnetic monopole. Therefore, also in our approach, instead of the volume integral as manipulated in section 3.1, the surface integral is introduced to evaluate the discretized rotation at the centroid or the edges of the element, i.e., at a non-collocated

grid. The discretization formulae for the toroidal component, the normal and the tangential components to the triangular edge are separately presented in the following subsections.

3.5.1. Toroidal Component

The surface integral for the toroidal component (ϕ-component) of the rotation in the element i is given by

$$\begin{aligned}
&\int_{S_i} (\nabla \times \mathbf{A}) \cdot \mathbf{e}_\phi dS \\
&= \int_{z_{S_i}} \int_{R_{S_i}} (\frac{\partial A_R}{\partial z} - \frac{\partial A_z}{\partial R}) dR dz \\
&= -\sum_n e^{\mathcal{I}n\phi} \oint_{l_i} (\tilde{\mathbf{A}}_n \cdot \mathbf{t}) dl,
\end{aligned}$$

and thus, the discretized formula for the surface integral is written by

$$\int_{S_i} (\nabla \times \mathbf{A}) \cdot \mathbf{e}_\phi dS = -\sum_n e^{\mathcal{I}n\phi} \sum_e \tilde{\mathbf{A}}_{e,n} \cdot \mathbf{t}_{e,n} \Delta l_e, \tag{19}$$

where the unit vector tangent to the edge $\mathbf{t}_e = \mathbf{n}_e \times \mathbf{e}_\phi$. Here, we approximate the averaged rotation in the element as

$$\int_{S_i} (\nabla \times \mathbf{A}) \cdot \mathbf{e}_\phi dS = \sum_n e^{\mathcal{I}n\phi} (\widetilde{\nabla \times \mathbf{A}})_{\phi_{i,n}} S_i. \tag{20}$$

Therefore, from equations (19) and (20), the toroidal component of the rotation is discretized as

$$(\widetilde{\nabla \times \mathbf{A}})_{\phi_{i,n}} = -\frac{1}{S_i} \sum_e \tilde{\mathbf{A}}_{e,n} \cdot \mathbf{t}_e \Delta l_e. \tag{21}$$

As you find the derivation and the form of equation (21), the toroidal component of the rotation is evaluated without the effect of the torus geometry. Therefore, in the straight limit, the evaluation of this component will not be transformed.

3.5.2. Poloidal Component (Normal Component)

In order to maintain the divergence free condition, the poloidal component of the rotation is defined at the edge of the triangular element. Thus, the rotation normal to the edge is integrated within the curved surface formed by the $\Delta\phi$ rotation of the edge, as shown in Figure 3 sketched by the shaded area:

$$\begin{aligned}
&\int_{S_{ne}} (\nabla \times \mathbf{A}) \cdot \mathbf{n} dS_n \\
&= \int_0^{\Delta\phi} \int_{e-}^{e+} R\{\mathrm{n}_R(\frac{1}{R}\frac{\partial A_z}{\partial \phi} - \frac{\partial A_\phi}{\partial z}) + \mathrm{n}_z(\frac{1}{R}\frac{\partial (RA_\phi)}{\partial R} - \frac{1}{R}\frac{\partial A_R}{\partial \phi})\} dl d\phi \\
&= \sum_n \Delta\phi \int_{e-}^{e+} \{\mathrm{n}_R(\mathcal{I}n\widetilde{A}_{zn} - \frac{\partial (R\widetilde{A}_{\phi_n})}{\partial z}) + \mathrm{n}_z(\frac{\partial (R\widetilde{A}_{\phi_n})}{\partial R} - \mathcal{I}n\widetilde{A}_{Rn})\} dl \\
&= \sum_n \Delta\phi \{\mathcal{I}n \int_{e-}^{e+} (\mathrm{t}_R\widetilde{A}_{Rn} + \mathrm{t}_z\widetilde{A}_{zn}) dl - \int_{e-}^{e+} (\mathrm{t}_R\frac{\partial}{\partial R} + \mathrm{t}_z\frac{\partial}{\partial z})(R\widetilde{A}_{\phi_n}) dl\} \\
&= \sum_n \Delta\phi \{\mathcal{I}n\tilde{\mathbf{A}}_{e,n} \cdot \mathbf{t}_e \Delta l_e - \int_{e-}^{e+} \frac{\partial (R\widetilde{A}_{\phi_n})}{\partial l} dl\} \\
&= \sum_n \Delta\phi \{\mathcal{I}n\tilde{\mathbf{A}}_{e,n} \cdot \mathbf{t}_e \Delta l_e - (R\widetilde{A}_\phi)_{e+,n} + (R\widetilde{A}_\phi)_{e-,n}\},
\end{aligned} \tag{22}$$

where $e+$ and $e-$ are the forward ($\mathbf{t}_e$-direction) and the backward ($-\mathbf{t}_e$-direction) vertices to the edge e, respectively. Similarly to the previous procedure, the normal component of the rotation is averaged out on the surface as

$$\int_{S_{\mathrm{n}e}} (\nabla \times \mathbf{A}) \cdot \mathbf{n} dS_{\mathrm{n}} = \sum_n \Delta\phi R_e (\widetilde{\nabla \times \mathbf{A}})_{\mathrm{n}_{e,n}} \Delta l_e, \tag{23}$$

and therefore, by comparing (22) with (23), we obtain the discretization for the normal component of the rotation as

$$(\widetilde{\nabla \times \mathbf{A}})_{\mathrm{n}_{e,n}} = \frac{\mathcal{I}n}{R_e} \tilde{\mathbf{A}}_{e,n} \cdot \mathbf{t}_e - \frac{(\widetilde{RA_\phi})_{e+,n} - (\widetilde{RA_\phi})_{e-,n}}{R_e \Delta l_e}. \tag{24}$$

Here we note that quantities $(\widetilde{RA_\phi})_{e\pm,n}$ at the vertices, those are derived from $\widetilde{RA_\phi}$ in neighbor elements, are needed for the evaluation of the rotation. In this study, $\widetilde{RA_\phi}$ is assumed to be linearly distributed in the element in order to keep the second-order accuracy. Therefore, the contribution of $(\widetilde{RA_\phi})_{j,n}$ at the neighbor element j to $(\widetilde{RA_\phi})_{e\pm,n}$ is expressed as $(\widetilde{RA_\phi})_{j(e\pm),n} = (\widetilde{RA_\phi})_{j,n} + \nabla(\widetilde{RA_\phi})_{j,n}(\mathbf{r}_{e\pm} - \mathbf{r}_{j,n})$. Subsequently, those of the adjacent elements to the vertex are averaged out as

$$(\widetilde{RA_\phi})_{e\pm,n} \equiv \frac{1}{n_{e\pm}} \sum_j \{(\widetilde{RA_\phi})_{j,n} + \nabla(\widetilde{RA_\phi})_{j,n} \cdot (\mathbf{r}_{e\pm} - \mathbf{r}_j)\}, \tag{25}$$

where $n_{e\pm}$ indicates the number of the elements j adjoining the vertex $e\pm$. For the case without the toroidal effect, these formulae are transformed as

$$(\widetilde{\nabla \times \mathbf{A}})_{\mathrm{n}_{e,n}} = \mathcal{I}n \tilde{\mathbf{A}}_{e,n} \cdot \mathbf{t}_e - \frac{\widetilde{A_y}_{e+,n} - \widetilde{A_y}_{e-,n}}{\Delta l_e}, \tag{26}$$

where

$$\widetilde{A_y}_{e\pm,n} \equiv \frac{1}{n_{e\pm}} \sum_j \{\widetilde{A_y}_{j,n} + \nabla \widetilde{A_y}_{j,n} \cdot (\mathbf{r}_{e\pm} - \mathbf{r}_j)\}. \tag{27}$$

3.5.3. Poloidal Component (Tangential Component)

The poloidal component of the rotation consists of two independent components. Those components were separately defined at a non-collocated grid as the normal components in the previous non-collocated approaches, as sketched in Figure 4 for instance. Although, on the cartesian grid or the structured grid in general, those types of the numerical scheme can be constructed straightforwardly, the discretization by similar procedures cannot be applied in the present triangular grid or the unstructured grid in general. Therefore, the other component in the poloidal plane must be defined at the triangular edge as the tangential component, where the normal component of the rotation is also defined.

Since we need to evaluate the tangential component of the rotation at the edge, the rotation must be integrated within the surface normal to $\mathbf{t}_e$. A simple idea occurs to us that the integration may be executed on the surface formed by the line connected with the centroids of the adjacent elements. However, though we can construct the polygons by connecting the adjacent centroids each other, the edge of the polygon neither crosses at right angle with the edge of the triangle nor intersects the triangular edge at a point of the center of both edges. Thus, here we integrate the rotation on the surface bounded by unknown integral limits $\pm\delta\mathrm{n}_e$

as depicted by shaded area in Figure 5:

$$
\begin{aligned}
&\int_{S_{te}} (\nabla \times \mathbf{A}) \cdot \mathbf{t} dS_{\mathrm{t}} \\
&= \int_0^{\Delta\phi} \int_{-\delta \mathrm{n}_e}^{+\delta \mathrm{n}_e} R\{\mathrm{t}_R(\frac{1}{R}\frac{\partial A_z}{\partial \phi} - \frac{\partial A_\phi}{\partial z}) + \mathrm{t}_z(\frac{1}{R}\frac{\partial (RA_\phi)}{\partial R} - \frac{1}{R}\frac{\partial A_R}{\partial \phi})\} d\mathrm{n} d\phi \\
&= \sum_n \Delta\phi \int_{-\delta \mathrm{n}_e}^{+\delta \mathrm{n}_e} \{\mathrm{t}_R(\mathcal{I}n\widetilde{A_{z}}_n - \frac{\partial (R\widetilde{A_{\phi}}_n)}{\partial z}) + \mathrm{t}_z(\frac{\partial (R\widetilde{A_{\phi}}_n)}{\partial R} - \mathcal{I}n\widetilde{A_{R}}_n)\} d\mathrm{n} \\
&= \sum_n \Delta\phi \{-\mathcal{I}n \int_{-\delta \mathrm{n}_e}^{+\delta \mathrm{n}_e} (\mathrm{n}_R \widetilde{A_R}_n + \mathrm{n}_z \widetilde{A_z}_n) d\mathrm{n} + \int_{-\delta \mathrm{n}_e}^{+\delta \mathrm{n}_e} (\mathrm{n}_R \frac{\partial}{\partial R} + \mathrm{n}_z \frac{\partial}{\partial z})(R\widetilde{A_\phi}_n) d\mathrm{n}\} \\
&= \sum_n \Delta\phi \{-\mathcal{I}n \tilde{\mathbf{A}}_{e,n} \cdot \mathbf{n}_e 2\delta \mathrm{n}_e + \int_{-\delta \mathrm{n}_e}^{+\delta \mathrm{n}_e} \frac{\partial (R\widetilde{A_\phi}_n)}{\partial \mathrm{n}} d\mathrm{n}\}, \qquad (28)
\end{aligned}
$$

where $-\delta \mathrm{n}_e$ and $+\delta \mathrm{n}_e$ are assumed to be placed in the adjacent elements i and j, respectively. Since the tangential rotation averaged on the surface is given by

$$
\int_{S_{te}} (\nabla \times \mathbf{A}) \cdot \mathbf{t} dS_{\mathrm{t}} = \sum_n \Delta\phi R_e (\widetilde{\nabla \times \mathbf{A}})_{\mathrm{t}_{e,n}} 2\delta \mathrm{n}_e, \qquad (29)
$$

we can partially discretize the toroidal component of the rotation as

$$
(\widetilde{\nabla \times \mathbf{A}})_{\mathrm{t}_{e,n}} = -\frac{\mathcal{I}n}{R_e} \tilde{\mathbf{A}}_{e,n} \cdot \mathbf{n}_e + \frac{1}{2R_e \delta \mathrm{n}_e} \int_{-\delta \mathrm{n}_e}^{+\delta \mathrm{n}_e} \frac{\partial (R\widetilde{A_\phi}_n)}{\partial \mathrm{n}} d\mathrm{n}. \qquad (30)
$$

In order to evaluate the rotation in the discretized system, the integral form of the last term in equation (30) is replaced by the algebraic function of the discretized quantities in neighbor elements. Here, since we approximate the distribution function of $R\widetilde{A_\phi}$ to the piecewise linear function in each element, the limits of the integral is separated for each distribution function as follows:

$$
\begin{aligned}
&\int_{-\delta \mathrm{n}_e}^{+\delta \mathrm{n}_e} \frac{\partial (R\widetilde{A_\phi}_n)}{\partial \mathrm{n}} d\mathrm{n} \\
&= \int_{+0}^{+\delta \mathrm{n}_e} \frac{\partial (R\widetilde{A_\phi}_n)}{\partial \mathrm{n}} d\mathrm{n} + \int_{-\delta \mathrm{n}_e}^{-0} \frac{\partial (R\widetilde{A_\phi}_n)}{\partial \mathrm{n}} d\mathrm{n} \\
&= \{(R\widetilde{A_\phi})_{+\delta \mathrm{n}_e} - (R\widetilde{A_\phi})_{+0}\} + \{(R\widetilde{A_\phi})_{-0} - (R\widetilde{A_\phi})_{-\delta \mathrm{n}_e}\} \\
&= \mathbf{n}_e \cdot \{\nabla (R\widetilde{A_\phi})_{j,n} + \nabla (R\widetilde{A_\phi})_{i,n}\} \delta \mathrm{n}_e.
\end{aligned}
$$

Thus, for any $\delta \mathrm{n}_e$, the integral term in equation (30) is simply replaced by the arithmetic mean of the gradients at the adjacent elements i and j. Also, in higher-order evaluations, the integral will be replaced by the mean of the gradients, those are evaluated more accurately than the present, at least in the limit of $\delta \mathrm{n}_e \to 0$. Finally, the tangential component of the rotation is derived as

$$
(\widetilde{\nabla \times \mathbf{A}})_{\mathrm{t}_{e,n}} = -\frac{\mathcal{I}n}{R_e} \tilde{\mathbf{A}}_{e,n} \cdot \mathbf{n}_e + \mathbf{n}_e \cdot \frac{\nabla (R\widetilde{A_\phi})_{j,n} + \nabla (R\widetilde{A_\phi})_{i,n}}{2R_e}, \qquad (31)
$$

and similarly, the discretization formula for non-curved version is give by

$$
(\widetilde{\nabla \times \mathbf{A}})_{\mathrm{t}_{e,n}} = -\mathcal{I}n \tilde{\mathbf{A}}_{e,n} \cdot \mathbf{n}_e + \mathbf{n}_e \cdot \frac{\nabla \widetilde{A_y}_{j,n} + \nabla \widetilde{A_y}_{i,n}}{2}. \qquad (32)
$$

3.5.4. Divergence of Discretized Rotation

The divergence of the rotation is calculated from equations (21), (24), and (13) in the torus geometry as follows:

$$
\begin{aligned}
& (\nabla \cdot \widetilde{\nabla \times \mathbf{A}})_{i,n} \\
= & \frac{1}{R_i S_i} \sum_e R_e (\nabla \widetilde{\times \mathbf{A}})_{e,n} \cdot \mathbf{n}_e \Delta l_e + \frac{\mathcal{I}n}{R_i} (\nabla \widetilde{\times \mathbf{A}})_{\phi i,n} \\
= & \frac{1}{R_i S_i} \sum_e R_e \{ \frac{\mathcal{I}n}{R_e} \tilde{\mathbf{A}}_{e,n} \cdot \mathbf{t}_e - \frac{(R\widetilde{A_\phi})_{e+,n} - (R\widetilde{A_\phi})_{e-,n}}{R_e \Delta l_e} \} \Delta l_e - \frac{\mathcal{I}n}{R_i S_i} \sum_e \tilde{\mathbf{A}}_{e,n} \cdot \mathbf{t}_e \Delta l_e \\
= & 0
\end{aligned}
$$

Thus, we can confirm the divergence free of the rotation at the triangular centroid i even numerically. The application of this condition to equation (4) leads that the divergence free constraint of the magnetic field is maintained throughout the simulation runs. Here we note that the tangential component is not needed for the evaluation of the divergence at the centroid. Also for the case without the toroidal effect, the divergence free condition of the rotation will be readily confirmed from equations (21), (26), and (14).

4. Boundary Conditions

In our method, the boundary grid is placed such that a face of the boundary element contacts with the boundary as shown in Figure 6. Under this boundary grid, the temporal evolution of the fluid components, ρ, $\rho\mathbf{V}$, and ϵ_F in the boundary element are determined both by the numerical fluxes for the fluid parts normal to each face including the boundary face and by the electromagnetic terms evaluated at the centroid. If the plasmas cannot flow in and out at the boundary wall, the fluid-related fluxes normal to the boundary are given as $\rho V_{\mathrm{n}_{eB}} = 0$, $\rho V_{\mathrm{n}_{eB}} V_{R_{eB}} + \mathrm{n}_{R_{eB}} P_{eB} = \mathrm{n}_{R_{eB}} P_{eB}$, $\rho V_{\mathrm{n}_{eB}} V_{\phi_{eB}} = 0$, $\rho V_{\mathrm{n}_{eB}} V_{z_{eB}} + \mathrm{n}_{z_{eB}} P_{eB} = \mathrm{n}_{z_{eB}} P_{eB}$, and $(\epsilon_{F_{eB}} + P_{eB}) V_{\mathrm{n}_{eB}} = 0$ for the continuity equation, the momentum equation of R-, ϕ-, z-components, and the energy equation, respectively, as far as the viscosity is very small. In order to know the rigid wall condition for the fluid-related fluxes completely, we must specify the pressure at the boundary wall. When the viscous effect on the boundary can be neglected, the wall condition gives the relation that $\mathbf{n}_{eB} \cdot \nabla P = \mathbf{n}_{eB} \cdot \mathbf{J} \times \mathbf{B}$. This relation is explicitly discretized as

$$
\frac{1}{R_i S_i} \{ R_{e1} \tilde{P}_{e1,n} (\mathbf{n}_{e1} \cdot \mathbf{n}_{eB}) \Delta l_{e1} + R_{e2} \tilde{P}_{e2,n} (\mathbf{n}_{e2} \cdot \mathbf{n}_{eB}) \Delta l_{e2} + R_{eB} \tilde{P}_{eB,n} \Delta l_{eB} \} = \mathbf{n}_{eB} \cdot (\widetilde{\mathbf{J} \times \mathbf{B}})_{eB,n},
$$

where $(\widetilde{\mathbf{J} \times \mathbf{B}})_{eB,n}$ is extrapolated or evaluated from the adjacent elements. Thus, the pressure at the boundary edge is determined.

We must also specify the boundary condition for the induction equation. The electric field tangent to the boundary wall, $E_{\phi_{eB\pm,n}}$ and $E_{teB,n}$, is fixed to be zero during a temporal evolution when the boundary wall is assumed to be a perfect conductor. The normal component, $E_{\mathrm{n}eB}$, is evaluated from which $E_{\mathrm{n}eB} = -V_{\phi_{eB}} B_{teB} + V_{teB} B_{\phi_{eB}}$, where the tangential components of the velocity at the boundary wall is either extrapolated from the adjacent elements or specified by zero as a no-slip condition.

5. Summary

We have presented new discretization formulae of the MHD equations based on both the finite volume in the poloidal plane and the spectral method for the differential to the toroidal direction.

In this approach, one can introduce the numerical scheme which constrains the divergence free condition of the rotation straightforwardly if the poloidal component of the rotation is evaluated at the triangular edges. Thus, we evaluated the poloidal component of the rotation at the edge under the assumption that RA_ϕ is the piecewise linear distribution function in each element. Also, the advantage of this approach is that no singular behavior appears in the magnetic axis or the separatrix without any special treatment. Indeed, as shown in Figure 7, plasmas flow across the near axis without any difficulty, where the flow of $n = 0$ mode is accelerated by the centrifugal force from the purely toroidal flow $V_{\phi,t=0} = V_0 \exp\{-\frac{(R-2)^2+z^2}{0.3^2}\}$. Here, the time integration was operated by the fourth-order Runge-Kutta-Gill method. The present numerical scheme will undergo more detail inspection on the accuracy of the numerical algorithm.

Now we are proceeding with the study for the linear and the nonlinear instabilities in high beta torus plasmas.

Acknowledgment

The authors would like to acknowledge Drs. M. Azumi and A. Funahashi at JAERI for their support in this work.

References

1. T. Ogino, R. J. Walker, and M. Ashour-Abdalla, *J. Geophys. Res.*, **99**, 11027 (1994).
2. T. Miyoshi and K. Kusano, *Geophys. Res. Lett.*, **24**, 2627 (1997).
3. W. Park, E. D. Fredrickson, A. Janos, J. Manickam, and W. M. Tang, *Phys. Rev. Lett.*, **75**, 1763 (1995).
4. R. G. Kleva and P. N. Guzdar, *Phys. Rev. Lett.*, **80**, 3081 (1998).
5. Y. Nishimura, J. D. Callen, and C. C. Hegna, *Phys. Plasmas*, **6**, 4685 (1999).
6. K. Kusano and T. Sato, *Nucl. Fusion*, **30**, 2075 (1990).
7. T. Hayashi, N. Mizuguchi, T-H. Watanabe, Y. Todo, T. Sato, and the Complexity Simulation Group, 17th IAEA Fusion Energy Conference, IAEA-TH3/3, 1998.
8. A. H. Glasser, C. R. Sovinec, R. A. Nebel, T. A. Gianakon, S. J. Plimpton, M. S. Chu, D. D. Schnack, and NIMROD Team, *Plasma Phys. Control. Fusion*, **41**, A747 (1999).
9. H. R. Strauss and W. Park, *Phys. Plasmas*, **7**, 250 (2000).
10. D. D. Schnack, I. Lottati, Z. Mikić, and P. Satyanarayana, *J. Comput. Phys*, **140**, 71 (1998).
11. D. Biskamp, E. Schwarz, and A. Celani, *Phys. Rev. Lett.*, **81**, 4855 (1998).
12. D. Biskamp and W.-C. Müller, *Phys. Rev. Lett.*, **83**, 2195 (1999).
13. R. E. Denton, J. F. Drake, and R. G. Kleva, *Phys. Fluids*, **30**, 1448 (1987).
14. J. Raeder, Proc. of the Fifth International School/Symposium for Space Simulations (RASC, Kyoto Univ.), 320, 1997.
15. C. R. Evans and J. F. Hawley, *Astrophys. J.*, **332**, 659 (1988).

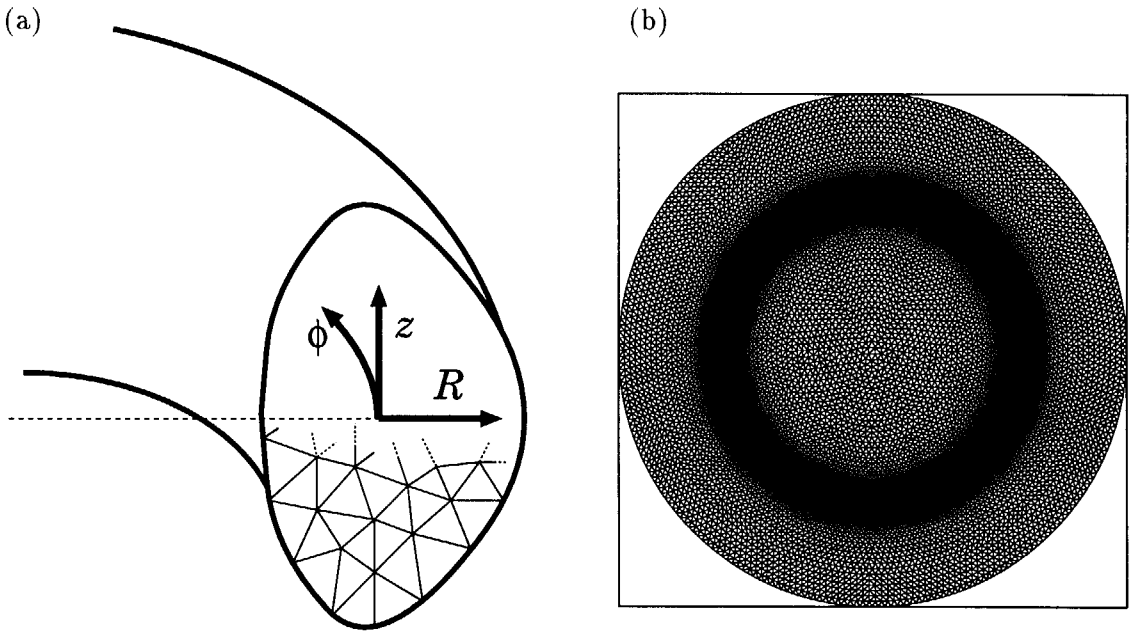

Figure 1: (a) The schematic diagram of the torus geometry where the poloidal plane is composed of arbitrary triangular elements. (b) An example of the unstructured grid composed of Delaunay triangles.

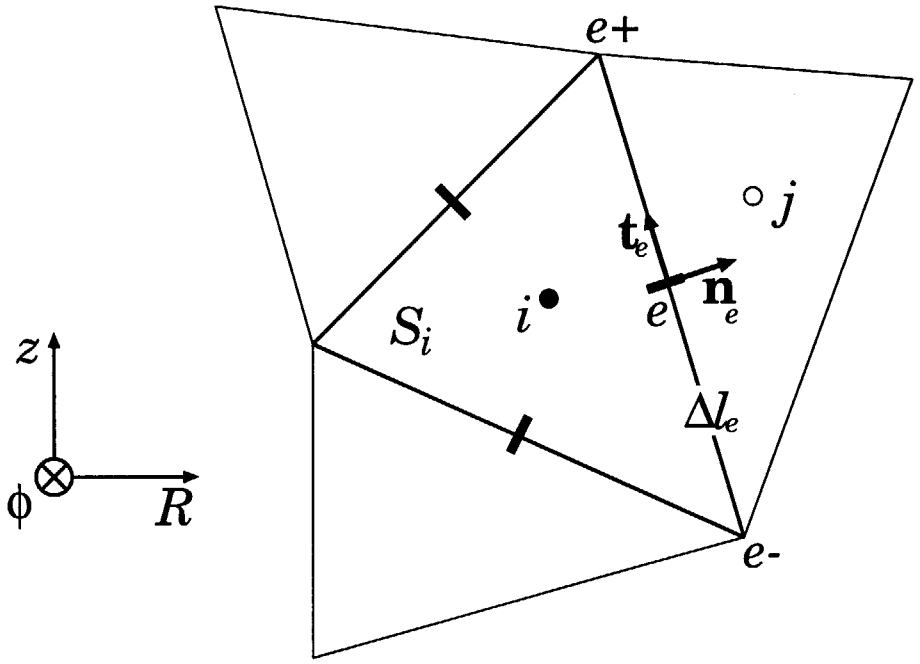

Figure 2: The necessary notations for the discretization specified by both the triangular element i and the relation with the adjacent element j.

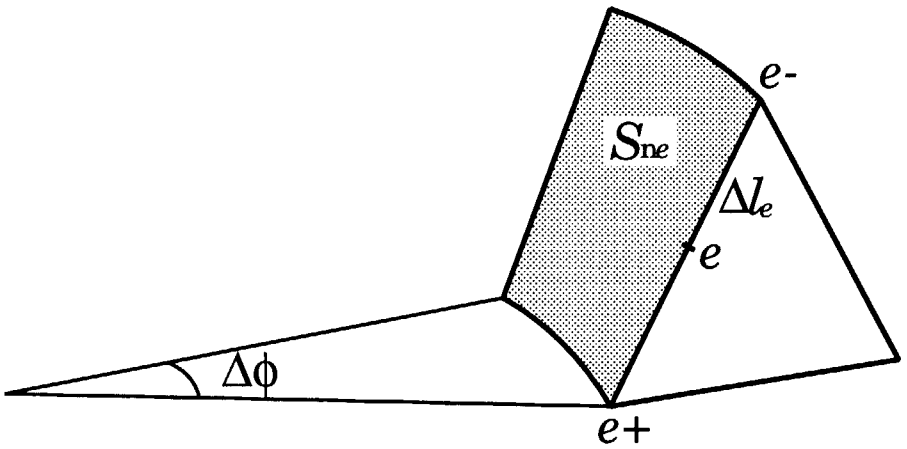

Figure 3: The integral area for the normal component of the rotation which is shown by a shaded region. The surface is formed by the locus of the edge.

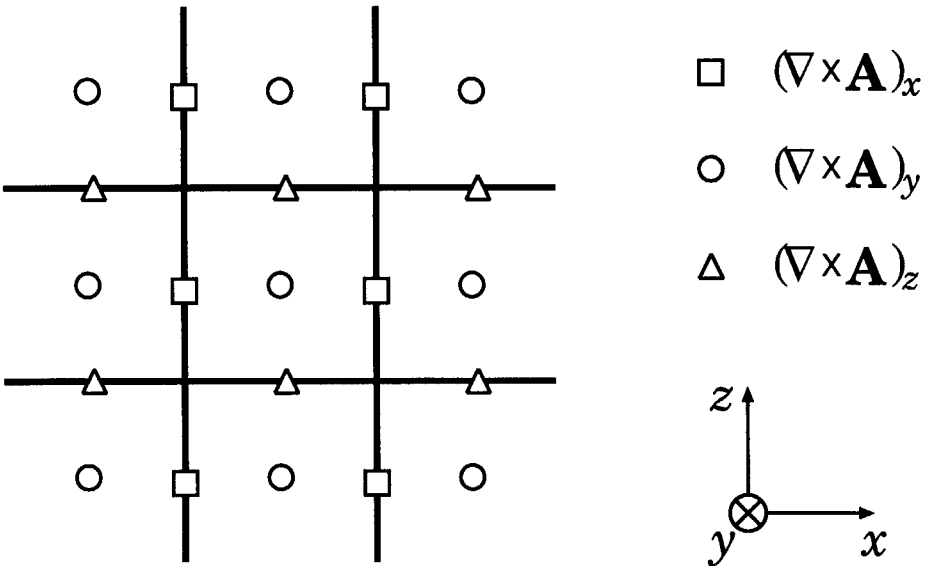

Figure 4: A non-collocated definition for each component of the rotation, where only the normal component is defined at the corresponding edge.

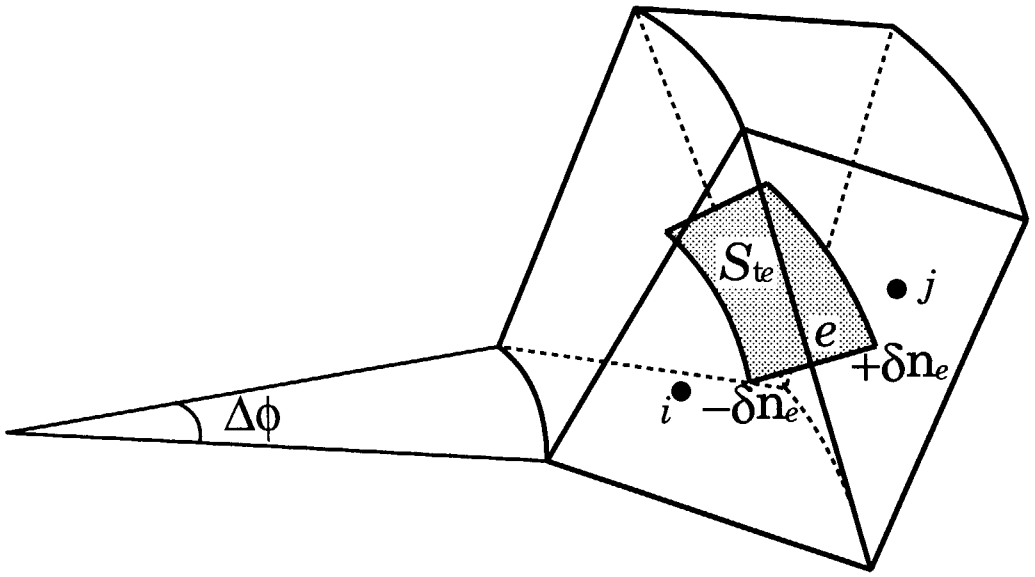

Figure 5: The integral area for the tangential component of the rotation which is shown by a shaded region. The surface is formed by the locus of the perpendicular line to the edge.

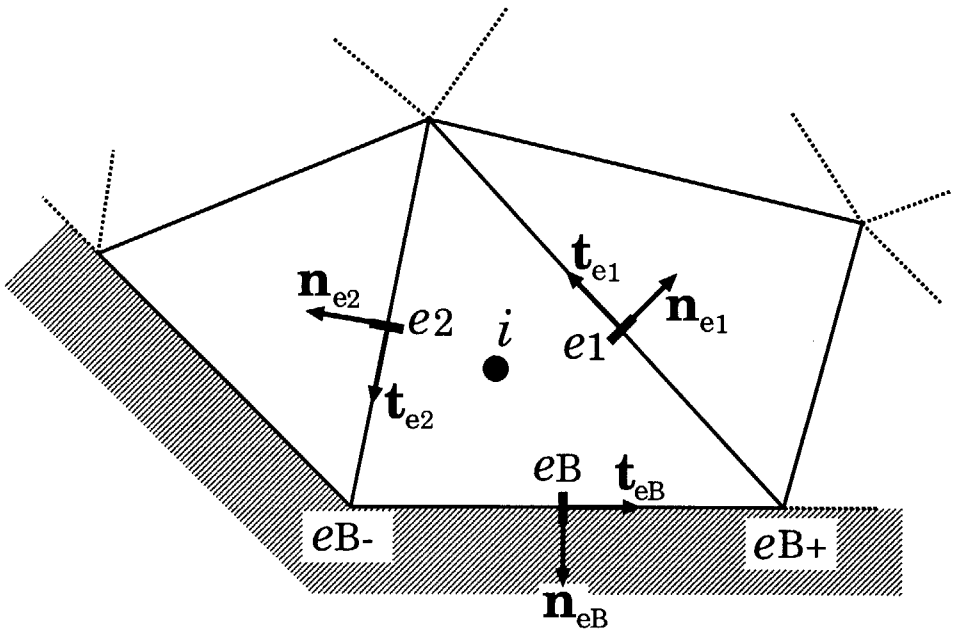

Figure 6: The distribution of the triangular elements adjacent to the boundary wall.

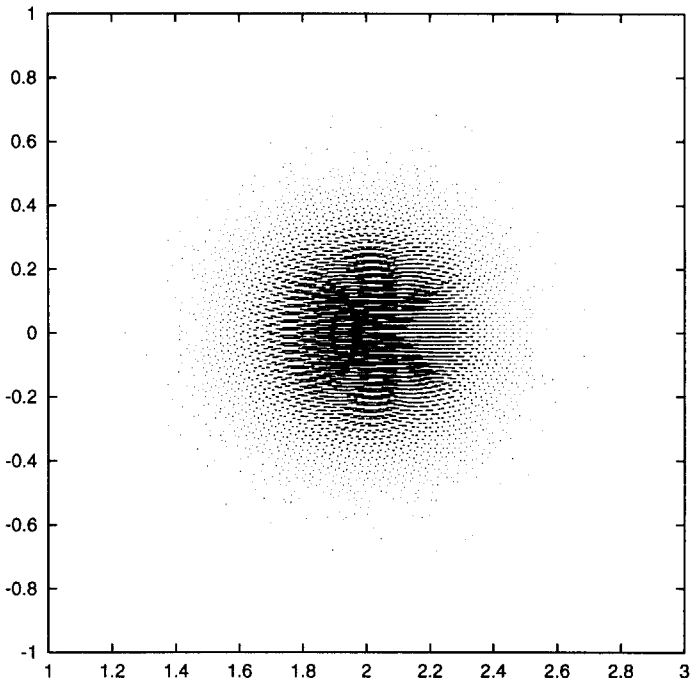

Figure 7: The poloidal plasma flow across the magnetic axis in the torus geometry with the aspect ratio $R_0/a = 2$.

This is a blank page.

国際単位系（SI）と換算表

表1　SI基本単位および補助単位

量	名称	記号
長さ	メートル	m
質量	キログラム	kg
時間	秒	s
電流	アンペア	A
熱力学温度	ケルビン	K
物質量	モル	mol
光度	カンデラ	cd
平面角	ラジアン	rad
立体角	ステラジアン	sr

表2　SIと併用される単位

名称	記号
分，時，日	min，h，d
度，分，秒	°，′，″
リットル	l，L
トン	t
電子ボルト	eV
原子質量単位	u

1 eV=1.60218×10^{-19}J

1 u=1.66054×10^{-27}kg

表3　固有の名称をもつSI組立単位

量	名称	記号	他のSI単位による表現
周波数	ヘルツ	Hz	s^{-1}
力	ニュートン	N	m·kg/s^2
圧力，応力	パスカル	Pa	N/m^2
エネルギー，仕事，熱量	ジュール	J	N·m
工率，放射束	ワット	W	J/s
電気量，電荷	クーロン	C	A·s
電位，電圧，起電力	ボルト	V	W/A
静電容量	ファラド	F	C/V
電気抵抗	オーム	Ω	V/A
コンダクタンス	ジーメンス	S	A/V
磁束	ウェーバ	Wb	V·s
磁束密度	テスラ	T	Wb/m^2
インダクタンス	ヘンリー	H	Wb/A
セルシウス温度	セルシウス度	C	
光束	ルーメン	lm	cd·sr
照度	ルクス	lx	lm/m^2
放射能	ベクレル	Bq	s^{-1}
吸収線量	グレイ	Gy	J/kg
線量等量	シーベルト	Sv	J/kg

表4　SIと共に暫定的に維持される単位

名称	記号
オングストローム	A
バーン	b
バール	bar
ガル	Gal
キュリー	Ci
レントゲン	R
ラド	rad
レム	rem

1 A=0.1nm=10^{-10}m

1 b=100fm^2=10^{-28}m^2

1 bar=0.1MPa=10^{5}Pa

1 Gal 1cm/s^2=10^{-2}m/s^2

1 Ci=3.7×10^{10}Bq

1 R=2.58×10^{-4}C/kg

1 rad 1cGy=10^{-2}Gy

1 rem=1cSv=10^{-2}Sv

表5　SI接頭語

倍数	接頭語	記号
10^{18}	エクサ	E
10^{15}	ペタ	P
10^{12}	テラ	T
10^{9}	ギガ	G
10^{6}	メガ	M
10^{3}	キロ	k
10^{2}	ヘクト	h
10^{1}	デカ	da
10^{-1}	デシ	d
10^{-2}	センチ	c
10^{-3}	ミリ	m
10^{-6}	マイクロ	μ
10^{-9}	ナノ	n
10^{-12}	ピコ	p
10^{-15}	フェムト	f
10^{-18}	アト	a

(注)

1．表1～5は「国際単位系」第5版，国際度量衡局1985年刊行による．ただし，1eVおよび1uの値はCODATAの1986年推奨値によった

2．表4には海里，ノット，アール，ヘクタールも含まれているが日常の単位なのでここでは省略した

3．barは，JISでは流体の圧力を表わす場合に限り表2のカテゴリーに分類されている

4．EC閣僚理事会指令ではbar，barnおよび「血圧の単位」mmHgを表2のカテゴリーに入れている

換　算　表

力	N(=10^{5}dyn)	kgf	lbf
	1	0.101972	0.224809
	9.80665	1	2.20462
	4.44822	0.453592	1

粘度　1Pa·s(N·s/m^2)=10P(ポアズ)(g/(cm·s))

動粘度　1m^2/s=10^{4}St(ストークス)(cm^2/s)

圧力	MPa(=10bar)	kgf/cm^2	atm	mmHg(Torr)	lbf/in^2(psi)
	1	10.1972	9.86923	7.50062×10^3	145.038
	0.0980665	1	0.967841	735.559	14.2233
	0.101325	1.03323	1	760	14.6959
	1.33322×10^{-4}	1.35951×10^{-3}	1.31579×10^{-3}	1	1.93368×10^{-2}
	6.89476×10^{-3}	7.03070×10^{-2}	6.80460×10^{-2}	51.7149	1

エネルギー・仕事・熱量	J(=10^7 erg)	kgf·m	kW·h	cal(計量法)	Btu	ft·lbf	eV
	1	0.101972	2.77778×10^{-7}	0.238889	9.47813×10^{-4}	0.737562	6.24150×10^{18}
	9.80665	1	2.72407×10^{-6}	2.34270	9.29487×10^{-3}	7.23301	6.12082×10^{19}
	3.6×10^6	3.67098×10^5	1	8.59999×10^2	3412.13	2.65522×10^6	2.24694×10^{25}
	4.18605	0.426858	1.16279×10^{-6}	1	3.96759×10^{-3}	3.08747	2.61272×10^{19}
	1055.06	107.586	2.93072×10^{-4}	252.042	1	778.172	6.58515×10^{21}
	1.35582	0.138255	3.76616×10^{-7}	0.323890	1.28506×10^{-3}	1	8.46233×10^{18}
	1.60218×10^{-19}	1.63377×10^{-20}	4.45050×10^{-26}	3.82743×10^{-20}	1.51857×10^{-22}	1.18171×10^{-19}	1

1 cal＝4.18605J（計量法）

＝4.184J（熱化学）

＝4.1855J（15℃）

＝4.1868J（国際蒸気表）

仕事率　1PS(仏馬力)

＝75 kgf·m/s

＝735.499W

放射能	Bq	Ci
	1	2.70270×10^{-11}
	3.7×10^{10}	1

吸収線量	Gy	rad
	1	100
	0.01	1

照射線量	C/kg	R
	1	3876
	2.58×10^{-4}	1

線量当量	Sv	rem
	1	100
	0.01	1

(86年12月26日現在)

A Spatial Discretization of the MHD Equations Based on the Finite Volume – Spectral Method